

Nonlinear oscillation characteristics of magnetic microbubbles under acoustic and magnetic fields

Lixia Zhao(赵丽霞), Huimin Shi(史慧敏), Isaac Bello, Jing Hu(胡静), Chenghui Wang(王成会), and Runyang Mo(莫润阳)

Citation: Chin. Phys. B, 2022, 31 (**3**): 034302. DOI: 10.1088/1674-1056/ac1f01
Journal homepage: http://cpb.iphy.ac.cn; http://iopscience.iop.org/cpb

What follows is a list of articles you may be interested in

High-efficiency unidirectional wavefront manipulation for broadband airborne sound with a planar device

Yang Tan(谭杨), Bin Liang(梁彬), and Jianchun Cheng(程建春)
Chin. Phys. B, 2022, 31 (**3**): 034303. DOI: 10.1088/1674-1056/ac1e14

Deep learning for image reconstruction in thermoacoustic tomography

Qiwen Xu(徐启文), Zhu Zheng(郑铸), and Huabei Jiang(蒋华北)
Chin. Phys. B, 2022, 31 (**2**): 024302. DOI: 10.1088/1674-1056/ac0dab

Assessment of cortical bone fatigue using coded nonlinear ultrasound

Duwei Liu(刘度为), Boyi Li(李博艺), Dongsheng Bi(毕东生), Tho N. H. T. Tran, Yifang Li(李义方), Dan Liu(刘丹), Ying Li(李颖), and Dean Ta(他得安)
Chin. Phys. B, 2021, 30 (**9**): 094301. DOI: 10.1088/1674-1056/ac0db2

Axial acoustic radiation force on an elastic spherical shell near an impedance boundary for zero-order quasi-Bessel-Gauss beam

Yu-Chen Zang(臧雨宸), Wei-Jun Lin(林伟军), Chang Su(苏畅), and Peng-Fei Wu(吴鹏飞)
Chin. Phys. B, 2021, 30 (**4**): 044301. DOI: 10.1088/1674-1056/abca27

High-resolution bone microstructure imaging based on ultrasonic frequency-domain full-waveform inversion

Yifang Li(李义方), Qinzhen Shi(石勤振), Ying Li(李颖), Xiaojun Song(宋小军), Chengcheng Liu(刘成成), Dean Ta(他得安), and Weiqi Wang(王威琪)
Chin. Phys. B, 2021, 30 (**1**): 014302. DOI: 10.1088/1674-1056/abc7aa

---

Nonlinear oscillation characteristics of magnetic microbubbles under acoustic and magnetic fields

Lixia Zhao(赵丽霞)[1], Huimin Shi(史慧敏)[1], Isaac Bello[2], Jing Hu(胡静)[1], Chenghui Wang(王成会)[1], and Runyang Mo(莫润阳)[1,†]

[1] *Shaanxi Key Laboratory of Ultrasonics, School of Physics and Information Technology, Shaanxi Normal University, Xi'an* 710119, *China*
[2] *Department of Chemistry, Ahmadu Bello University, Zaria* 810001, *Nigeria*

(Received 30 April 2021; revised manuscript received 8 August 2021; accepted manuscript online 19 August 2021)

Microbubbles loaded with magnetic nanoparticles (MMBs) have attracted increasing interests in multimode imaging and drug/gene delivery and targeted therapy. However, the dynamic behaviors generated in diagnostic and therapeutic applications are not clear. In the present work, a novel theoretical model of a single MMB was developed, and the dynamic responses in an infinite viscous fluid were investigated under simultaneous exposure to magnetic and acoustic fields. The results showed that the amplitude reduces and the resonant frequency increases with the strength of the applied steady magnetic field and the susceptibility of the magnetic shell. However, the magnetic field has a limited influence on the oscillating. It is also noticed that the responses of MMB to a time-varying magnetic field is different from a steady magnetic field. The subharmonic components increase firstly and then decrease with the frequency of the magnetic field and the enhanced effect is related to the acoustic driving frequency. It is indicated that there may be a coupling interaction effect between the acoustic and magnetic fields.

Keywords: magnetic microbubbles, ultrasound, magnetic field, nonlinear oscillation

PACS: 43.25.+y, 43.35.+d **DOI:** 10.1088/1674-1056/ac1f01

1. Introduction

Ultrasound contrast agents (UCAs) can not only improve the contrast of images, but also show great potential in molecular imaging and drug/gene delivery.[1] The use of ultrasound in combination with drug-loaded microbubbles offers considerable potential for the targeted treatment of a wide range of diseases including several types of cancer.[2] It is well known that UCAs are generally injected into the body through intravenous injections and delivered to the lesion site through blood circulation.[3] The extravasation of the drug during the circulatory delivery causes damage to other organs, and it is also not conducive for drug aggregation in the target area.[4] To achieve sufficient concentration at the targeted location, Zhang *et al.*[5] used drug-loaded microbubbles for targeted therapy and showed that antibody-targeted therapy effectively raise the inhibition rate of the tumor cells *in vivo*. Microbubbles can also accumulate at the lesion site through the action of acoustic radiation force to achieve the purpose of treatment.[6] However, this method strongly depends on the conditions of blood flow and low concentration of microbubbles due to the blood flow will potentially decrease the targeting rate. To solve this problem, a potential strategy which has been demonstrated is to use microbubbles loaded with magnetics nanoparticles (MNPs) and form magnetic microbubbles (MMBs).[7] MMBs maintain the volume oscillation properties in moderate acoustic fields[8,9] and possess sensitivity to magnetic fields, whose location can be manipulated by an externally applied magnetic field. Magnetic field can weaken the strength of sonoluminescence in water under a fixed magnetic field, the sweep acoustic field results of Young[10] showed that the upper and lower bound of the forced pressure in the sonoluminescence region increased significantly with the magnetic field. The ability of MMBs to enhance the contrast of ultrasound/magnetic resonance images has been confirmed by many experiments.[11–14] The use of MMBs in therapeutic applications, in particular drug delivery and gene therapy has become a highly active area of research. Recently, Zhang *et al.*[15] utilized MMBs for ultrasound thrombolysis under a rotational magnetic field in different clot conditions and different clot ages (fresh, retracted) to improve the thrombolysis efficiency. Owen *et al.*[16] indicated that lipid-coated MMBs could be retained with a magnet against clinically relevant flow conditions. MMB can enhanc gene transfection has been demonstrated *in vitro* and *in vivo* by Stride.[2,14] However, the mechanisms of MMBs enhancement transfection rates are not clear. One hypothesis is that the external magnetic field causes a higher concentration of MMBs at the target site and ensures sufficient proximity between bubbles and target cells.[14]

In fact, the lack of a deep understanding of the dynamics of MMBs in the magneto-acoustic combined field has greatly limited their novel design and clinical application.[9] Further investigation to fully understand the mechanism of enhancement and, hence, optimize the delivery protocols is required. It is necessary to explore an innovation dynamic model and characterize the effects of MNPs on its dynamic and acoustic-magnetic responses of single MMB. Previous re-

†Corresponding author. E-mail: mmrryycn@snnu.edu.cn

© 2022 Chinese Physical Society and IOP Publishing Ltd

search has transformed the dynamics of MMBs into another problem: the dynamics of one or more non-magnetic bubbles within highly magnetic fluids.[17] Based on this approach, Malvar *et al.*[18] studied the dynamics of a spherical bubble in a magnetic fluid by a new version of the Rayleigh–Plesset equation, and pointed out that the bubble oscillatory motion can be controlled and its collapse can be avoided when a high magnetic is applied. The experiment data of external magnetic field modulation on bubble acoustic oscillation can be obtained by induction sensor and piezoelectric element, respectively.[19] Mulvana *et al.*[20] modified the Church model[21] under the assumptions that the magnetic shell is a hydrophobic viscous fluid with uniformly distributed spherical magnetic nanoparticles, and the effects of the volume fraction of magnetic nanoparticles on the shell density was considered. Zhao *et al.*[22] considered the influence of the volume fraction of MNPs on the viscosity of the fluid layer, and then analyzed the vibration behavior of MMBs only in the presence of an acoustic field.

The above alternative method, which treated single MMB as a nonmagnetic bubble in magnetic fluid, is indirect. In this work, a novel mathematical model is developed to study the dynamic behavior of a MMB under a combined magneto-acoustic field. A MMB is modelled as a air-filled sphere and surrounded by a double-layer membrane, which coupled with magnetic nanoparticles, and the influence of MNPs on the viscosity of magnetic fluid was considered. Furthermore, dimensionless parameters such as magnetic Reynolds number were used to make a dimensionless and linear analysis of the dynamic equation. The effects of magnetic physical parameters and acoustic parameters on the dynamics of the MMB was investigated to provide useful insights in previous studies.

2. Theoretical model

The structural model of a MMB is shown in Fig. 1. The inner (1) is air and outer (3) is a hydrophobic phospholipid layer. The shell (2) is magnetic fluid layer (MFL) and it is consisted with hydrophobic oleic acid uniformly distributed with superparamagnetic iron oxide (SPIOs) nanoparticles. In previous reports, SPIOs were always used for incorporating MMBs and the sizes were generally from nanometers to tens of nanometers and then the MMBs would have a fast response to the external magnetic field.[9,11] The magnetic response of the MMB were affected by the volume fraction of SPIOs in magnetic fluid.[23,24] The initial inner and outer radius of the MMB are R_{10} and R_{20}, respectively. The thickness of layer (3) is much smaller than (2) and it is negligible. Both MF and the ambient liquid outside the bubble are incompressible Newtonian fluids and (ρ_s, η_s) and (ρ_l, η_l) are their density and viscosity, respectively. The viscosity of the phospholipid layer is η_{s0}. The density of SPIOs particles is ρ_{np}, the volume fraction is generally less than 0.1[24] and the interaction between particles is negligible. The MMB was subjected to an combined external fields, which include a sine wave sound field p_d ($p_d = p_a \sin 2\pi ft$) and an applied magnetic field with intensity H. The magnetic field far from the bubble should approach the uniform field and the component in the z axis is $H_0\boldsymbol{k}$.

This study is concerned primarily with the dynamic and acoustic-magnetic response of individual MMB. It is well accepted that US-induced stable and inertial cavitation plays an important role in the development of microbubble-assisted diagnostic and therapeutic application. However, it is very difficult to develop a mathematical model to describe non-spherical bubble due to the complexity responses in a combined magneto-acoustic field and more sophisticated numerical techniques. To simplify the problem, the effects of bubble translation under flow, acoustic radiation force or due to a magnetic field are neglected since these will occur on a relatively long timescale. Meanwhile, the non-spherical deformation of the vibrating bubble is ignored here. Assume that MMB only vibrates in the radial direction and remains spherical during expansion and contraction[25] and regardless of the mass exchange between the inside and outside of the membrane.

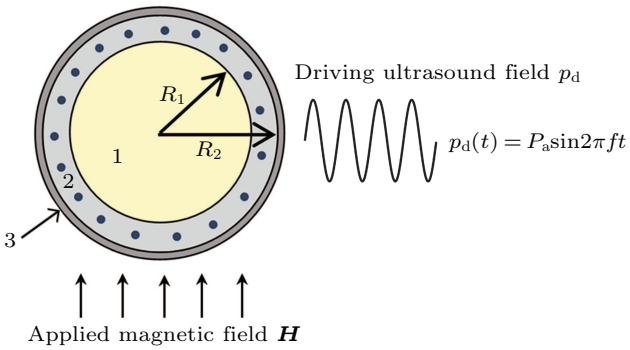


Fig. 1. Schematic of single MMB with acoustic p_d and magnetic ($\boldsymbol{H} = H_0\boldsymbol{k}$) applied field. (1-air, 2-magnetic fluid layer, 3-phospholipid thin layer).

The balance of momentum for the continuous medium is given by[24]

$$\rho\left(\frac{\partial \boldsymbol{v}}{\partial t} + \boldsymbol{v}\cdot\nabla\boldsymbol{v}\right) = -\nabla p + \nabla\cdot\boldsymbol{\sigma}, \tag{1}$$

where ρ, v, p, and σ are the density, the velocity, the pressure, and the viscous stress tensor of the medium, respectively.

The radial components of the momentum equation can be written as

$$\rho\left(\frac{\partial v}{\partial t} + v\frac{\partial v}{\partial r}\right) = \frac{\partial p}{\partial r} + \frac{1}{r^2}\frac{\partial}{\partial r}\left(r^2\sigma_{rr}\right) + \frac{\sigma_{rr}}{r}. \tag{2}$$

The boundary conditions at R_1 and R_2 are given, respectively, by

$$P_G(R_1,t) = P_S(R_1,t) - \sigma_{S,rr}(R_1,t) + \frac{2\sigma_1}{R_1} \quad (r = R_1), \tag{3}$$

$$P_s(R_2,t) - \sigma_{S,rr}(R_2,t) = P_L(R_2,t) - \sigma_{L,rr}(R_2,t) + \frac{2\sigma_2}{R_2} + 4\eta_{s0}\frac{\dot{R}_2}{R_2^2}$$

$$+\frac{2K}{R_2}\left(1-\left(\frac{R_{20}}{R_2}\right)^2\right) \quad (r=R_2), \tag{4}$$

where $P_{\rm G}(R_1,t)=P_{\rm G0}(R_{10}/R_1)^{3\gamma}$, $P_{\rm G}(R_1,t)$ is the internal gas pressure, $P_{\rm G0}$ is the initial equilibrium gas pressure in the bubble, σ_1 and σ_2 are internal and external surface tension coefficients, respectively. γ is the ratio of specific heats. $P_{\rm S}(R_1,t)$ and $P_{\rm S}(R_2,t)$ are the pressures at R_1 and R_2, respectively, and $\sigma_{{\rm S},rr}$ and $\sigma_{{\rm L},rr}$ are the radial stress components of the fluid inside and outside the film, respectively. The last two items on the right are the viscosity term and the surface tension change term[20] caused by the outer phospholipid layer. $\eta_{\rm s0}$ is the surface viscosity coefficient and K is a constant of the phospholipid layer.

Substituting Eqs. (3) and (4) into Eq. (2) and integrating it over r from R_1 to R_2 by using the parameters of magnetic fluid film and from R_2 to ∞ by using the parameters of the surrounding infinite liquid, we obtain

$$\begin{aligned}
&R_1\ddot{R}_1\left[1+\left(\frac{\rho_{\rm l}-\rho_{\rm s}}{\rho_{\rm s}}\right)\frac{R_1}{R_2}\right]\\
&+\dot{R}_1^2\left[\frac{3}{2}+\left(\frac{\rho_{\rm l}-\rho_{\rm s}}{\rho_{\rm s}}\right)\left(\frac{4R_2^3-R_1^3}{2R_2^3}\right)\left(\frac{R_1}{R_2}\right)\right]\\
&=\frac{1}{\rho_{\rm s}}\left[P_{\rm G0}\left(\frac{R_{10}}{R_1}\right)^{3\gamma}-P_\infty-\frac{2\sigma_1}{R_1}-\frac{2\sigma_2}{R_2}-\frac{4\eta_{\rm s0}\dot{R}_2}{R_2^2}-\frac{2K}{R_2}\right.\\
&\left.\times\left(1-\left(\frac{R_{20}}{R_2}\right)^2\right)+3\int_{R_1}^{R_2}\frac{\sigma_{{\rm S},rr}}{r}{\rm d}r+3\int_{R_2}^{\infty}\frac{\sigma_{{\rm L},rr}}{r}{\rm d}r\right].
\end{aligned} \tag{5}$$

In Eq. (5), $\sigma_{{\rm S},rr}$ contains viscous and magnetic stress radial components in MFL, while $\sigma_{{\rm L},rr}$ represents the viscous stress component in surrounding liquid. $\sigma_{{\rm S},rr}$ can be expressed as

$$\sigma_{{\rm S},rr}=\sigma_{{\rm S},rr}^{\rm vis}+\sigma_{{\rm S},rr}^{\rm mag}. \tag{6}$$

Since the MFL and the surrounding fluid are both incompressible viscous Newtonian fluids, if the viscosity of the liquid is η, the radial component of the particle velocity is v_r, and radial component of the viscous stress tensor $\sigma_{rr}^{\rm vis}$ can be calculated by

$$\sigma_{rr}^{\rm vis}=2\eta\frac{\partial v_r}{\partial r},\quad v_r=\frac{1}{r^2}R_1^2\dot{R}_1. \tag{7}$$

Then, $\sigma_{rr}^{\rm vis}$ can be written as

$$\sigma_{rr}^{\rm vis}=2\eta\left(-2\frac{R_1^2\dot{R}_1}{r^3}\right)=-4\eta\frac{R_1^2\dot{R}_1}{r^3}. \tag{8}$$

Therefore,viscous stress tensor of surrounding infinite liquid $\sigma_{{\rm L},rr}^{\rm vis}$ can be written as

$$\sigma_{{\rm L},rr}^{\rm vis}=-4\eta_{\rm L}\frac{R_1^2\dot{R}_1}{r^3}. \tag{9}$$

By using Eq. (9), the integral term of the viscous stress tensor of surrounding liquid in Eq. (5) can be written as

$$\begin{aligned}
3\int_{R_2}^{\infty}\frac{\sigma_{{\rm L},rr}^{\rm vis}}{r}{\rm d}r&=3\int_{R_2}^{\infty}-4\eta_{\rm L}\frac{R_1^2\dot{R}_1}{r^4}{\rm d}r=4\eta_{\rm L}R_1^2\dot{R}_1r^{-3}\Big|_{R_2}^{\infty}\\
&=-4\eta_{\rm L}\frac{R_1^2\dot{R}_1}{R_2^3}.
\end{aligned} \tag{10}$$

Viscous stress tensor of the MFL can also be written as

$$\sigma_{{\rm S},rr}^{\rm vis}=-4\eta_{\rm S}\frac{R_1^2\dot{R}_1}{r^3}. \tag{11}$$

By using Eq. (11), the integral term of the viscous stress tensor of the magnetic liquid layer in Eq. (5) can be written as

$$\begin{aligned}
3\int_{R_1}^{R_2}\frac{\sigma_{{\rm S},rr}^{\rm vis}}{r}{\rm d}r&=3\int_{R_1}^{R_2}-4\eta_{\rm S}\frac{R_1^2\dot{R}_1}{r^4}{\rm d}r=4\eta_{\rm S}R_1^2\dot{R}_1r^{-3}\Big|_{R_1}^{R_2}\\
&=-4\eta_{\rm S}\frac{V_{\rm S}\dot{R}_1}{R_2^3R_1}.
\end{aligned} \tag{12}$$

In addition, magnetic stress tensor $\boldsymbol{\sigma}$ can be expressed as[18]

$$\boldsymbol{\sigma}=-\frac{1}{2}\mu_0H^2\boldsymbol{I}+\boldsymbol{HB}, \tag{13}$$

where μ_0 is the magnetic permeability of vacuum, and $\boldsymbol{I}$ is the identity tensor. The relationship of the magnetic stress tensor is expressed in Kelvin–Maxwell force per unit volume as $\boldsymbol{F}_m=\mu_0\boldsymbol{M}\cdot\nabla\boldsymbol{H}$. Magnetization, $\boldsymbol{M}$, is parallel to the magnetic field $\boldsymbol{H}$, and $\boldsymbol{B}$ is the magnetic field strength. In the case of superparamagnetic fluid, $\boldsymbol{H}$ and $\boldsymbol{B}$ satisfy Maxwell's equations

$$\nabla\times\boldsymbol{H}=0,\quad \nabla\cdot\boldsymbol{B}=0. \tag{14}$$

It can be seen from Eq. (13) that an applied magnetic field can change the stress tensor components of the magnetic fluid film, and $\boldsymbol{H}$ is calculated from $\boldsymbol{H}=-\nabla\psi$, where ψ is the magnetic potential and satisfies the Laplace's equation in the axisymmetric spherical coordinate system $\nabla^2\psi=0$, that is,

$$\frac{\partial}{\partial r}\left(r^2\frac{\partial\psi}{\partial r}\right)+\frac{1}{\sin\theta}\frac{\partial}{\partial\theta}\left(\sin\theta\frac{\partial\psi}{\partial\theta}\right)=0. \tag{15}$$

According to the boundary value conditions[25]

$$\begin{aligned}
\psi_1|_{R=R_1}&=\psi_2|_{R=R_1},\quad \mu_0H_{1n}=\mu H_{2n},\\
\psi_2|_{R=R_2}&=\psi_3|_{R=R_2},\quad \mu H_{2n}=\mu_0H_{3n},
\end{aligned} \tag{16}$$

an analytical solution of the magnetic potential ψ in Eq. (15) can be obtained as

$$\psi=\begin{cases}
ar\cos\theta, & (r<R_1),\\
\left(br+\dfrac{c}{r^2}\right)\cos\theta, & (R_1<r<R_2),\\
\left(-H_0r+\dfrac{d}{r^2}\right)\cos\theta, & (r>R_2).
\end{cases} \tag{17}$$

In the spherical coordinate system,

$$\boldsymbol{H}=-\nabla\varphi=-\left(\frac{\partial\psi}{\partial r}\boldsymbol{e}_r+\frac{1}{r}\frac{\partial\psi}{\partial\theta}\boldsymbol{e}_\theta\right). \tag{18}$$

Then $\boldsymbol{H}$ can be written as

$$\boldsymbol{H}=\begin{cases}-a\left(\cos\theta\boldsymbol{e}_r-\sin\theta\boldsymbol{e}_\theta\right), & (r<R_1),\\ \left(\dfrac{2c}{r^3}-b\right)\cos\theta\boldsymbol{e}_r+\left(b+\dfrac{c}{r^3}\right)\sin\theta\boldsymbol{e}_\theta, & (R_1<r<R_2),\\ -\left(-H_0-\dfrac{2d}{r^3}\right)\cos\theta\boldsymbol{e}_r+\left(-H_0+\dfrac{d}{r^3}\right)\sin\theta\boldsymbol{e}_\theta, & (r>R_2).\end{cases}\tag{19}$$

If the suface current generated on the SPIOs due to MMB vibration is ignored, the magnetic field is continuous through the bubble interface, and the coefficients a, b, c, and d are given by

$$\begin{aligned}a&=-\frac{9\mu\mu_0H_0R_2^3}{(2\mu+\mu_0)(2\mu_0+\mu)R_2^3-2(\mu-\mu_0)^2R_1^3},\\ b&=-\frac{3\mu_0(\mu_0+2\mu)R_2^3H_0}{(2\mu+\mu_0)(2\mu_0+\mu)R_2^3-2(\mu-\mu_0)^2R_1^3},\\ c&=-\frac{3\mu_0(\mu-\mu_0)H_0R_1^3R_2^3}{(2\mu+\mu_0)(2\mu_0+\mu)R_2^3-2(\mu-\mu_0)^2R_1^3},\\ d&=\frac{H_0R_2^3\left(R_2^3-R_1^3\right)(\mu-\mu_0)(2\mu+\mu_0)}{(2\mu+\mu_0)(2\mu_0+\mu)R_2^3-2(\mu-\mu_0)^2R_1^3}.\end{aligned}\tag{20}$$

Moreover, the magnetization intensity H of the magnetic fluid is not equal to zero, so the magnetic induction $\boldsymbol{B}$ and $\boldsymbol{H}$ satisfy

$$\boldsymbol{B}=\mu_0(\boldsymbol{H}+\boldsymbol{M})=\mu_0(1+\chi)\boldsymbol{H},\tag{21}$$

where χ is the magnetic susceptibility of the material of MF layer. The radial scalar component of magnetic stress $\sigma_{rr}^{\mathrm{mag}}$ is given as[18]

$$\sigma_{rr}^{\mathrm{mag}}=-\frac{\mu_0}{2}\left(H_r^2+H_\theta^2\right)+\mu_0(1+\chi)H_r^2.\tag{22}$$

Since only the movement in the radial direction is considered, H_θ in the radial magnetic stress is calculated by the average value[26]

$$\frac{1}{2\pi}\int_0^{2\pi}\cos^2\theta=\frac{1}{2},\quad\frac{1}{2\pi}\int_0^{2\pi}\sin^2\theta=\frac{1}{2}.\tag{23}$$

When $R_1<r<R_2$, the radial magnetic field strength H_r and the tangential magnetic field strength H_θ are respectively

$$H_r=\left(\frac{2c}{r^3}-b\right)\cos\theta,\quad H_\theta=\left(b+\frac{c}{r^3}\right)\sin\theta.\tag{24}$$

Substituting Eqs. (23) and (24) into Eq. (22), $\sigma_{rr}^{\mathrm{mag}}$ can be obtained as

$$\begin{aligned}\sigma_{rr}^{\mathrm{mag}}&=-\frac{\mu_0}{2}\left(H_r^2+H_\theta^2\right)+\mu_0(1+\chi)H_r^2\\ &=\frac{\mu_0}{4r^6}\left(2b^2r^6\chi-2bc(3+4\chi)r^3+c^2(3+8\chi)\right).\end{aligned}\tag{25}$$

Substitute Eq. (20) into Eq. (25) and integrate over r to calculate the contribution of magnetic field to MMB.

In the part of MFL, $\sigma_{rr}^{\mathrm{mag}}$is substituted for $\sigma_{\mathrm{S},rr}^{\mathrm{mag}}$. The integral of $\sigma_{\mathrm{S},rr}^{\mathrm{mag}}$ from R_1 to R_2 by Eq. (5) is defined as the magnetic pressure and is denoted by G,

$$\begin{aligned}G&=3\int_{R_1}^{R_2}\frac{\sigma_{\mathrm{S},rr}^{\mathrm{mag}}}{r}\mathrm{d}r\\ &=-9H_0^2\mu_0^3\frac{f_1R_1^6-f_2R_1^3R_2^3+R_2^6}{f_4R_1^6-f_5R_1^3R_2^3+f_6R_2^6},\end{aligned}\tag{26}$$

where

$$\begin{aligned}f_1&=(3+8\chi)(\mu-\mu_0)^2,\\ f_2&=4(3+4\chi)(\mu-\mu_0)(2\mu+\mu_0),\\ f_3&=3\left(\mu^2\left(7+8\chi+16\chi In\frac{R_1}{R_2}\right)+2\mu\mu_0\left(8\chi In\frac{R_1}{R_2}-1\right)\right.\\ &\quad\left.+\mu_0^2\left(4\chi In\frac{R_1}{R_2}-8\chi-5\right)\right),\\ f_4&=32(\mu-\mu_0)^4,\\ f_5&=32(\mu-\mu_0)^2(\mu+2\mu_0)(2\mu+\mu_0),\\ f_6&=8\left(2\mu^2+5\mu\mu_0+2\mu_0^2\right)^2.\end{aligned}$$

Substituting Eqs. (10), (12), and (26) into Eq. (5) yields

$$\begin{aligned}&R_1\ddot{R}_1\left[1+\left(\frac{\rho_{\mathrm{l}}-\rho_{\mathrm{s}}}{\rho_{\mathrm{s}}}\right)\frac{R_1}{R_2}\right]\\ &+\dot{R}_1^2\left[\frac{3}{2}+\left(\frac{\rho_{\mathrm{l}}-\rho_{\mathrm{s}}}{\rho_{\mathrm{s}}}\right)\left(\frac{4R_2^3-R_1^3}{2R_2^3}\right)\left(\frac{R_1}{R_2}\right)\right]\\ &=\frac{1}{\rho_{\mathrm{s}}}\left[P_{\mathrm{G}0}\left(\frac{R_{10}}{R_1}\right)^{3\gamma}-P_\infty-\frac{2\sigma_1}{R_1}-\frac{2\sigma_2}{R_2}-\frac{4\eta_{\mathrm{s}0}\dot{R}_2}{R_2^2}-\frac{2K}{R_2}\right.\\ &\times\left.\left(1-\left(\frac{R_{20}}{R_2}\right)^2\right)-4\eta_{\mathrm{S}}\frac{V_{\mathrm{S}}\dot{R}_1}{R_2^3R_1}-4\eta_{\mathrm{L}}\frac{R_1^2\dot{R}_1}{R_2^3}+G\right].\end{aligned}\tag{27}$$

To facilitate the numerical analysis, we shall make use of the dimensionless parameters as follows:

$$\begin{aligned}&R_1=R_{10}r_1,\quad R_2=R_{20}r_2,\quad t^*=\frac{t}{t_{\mathrm{c}}},\quad U_{\mathrm{c}}=\sqrt{\frac{P_0}{\rho_{\mathrm{S}}}},\quad t_{\mathrm{c}}=\frac{R_{10}}{U_{\mathrm{c}}},\\ &\omega^*=\omega t_{\mathrm{c}},\quad A=\frac{P_{\mathrm{a}}}{P_0},\quad \mu_{\mathrm{r}}=\frac{\mu}{\mu_0},\quad R_{\mathrm{e}}=\frac{\rho_{\mathrm{S}}U_{\mathrm{c}}R_{10}}{\eta_{\mathrm{S}}},\\ &W_{\mathrm{e}}=\frac{\rho_{\mathrm{S}}U_{\mathrm{c}}^2R_{10}}{\sigma_1},\quad R_{\mathrm{e}}^{\mathrm{mag}}=\frac{\rho_{\mathrm{S}}U_{\mathrm{c}}^2}{\mu_0H_0^2},\quad R_{20}=\zeta R_{10},\quad \sigma_2=\varepsilon\sigma_1,\\ &\rho_{\mathrm{L}}=n\rho_{\mathrm{S}},\quad \eta_{\mathrm{L}}=q\eta_{\mathrm{S}},\quad \frac{\eta_{\mathrm{S}0}}{R_{10}}=m\eta_{\mathrm{S}},\quad K=l\sigma_1,\end{aligned}$$

where R_{10}, U_{c}, and t_{c} are characteristic length, velocity and time, respectively. The Reynolds number R_{e} indicates the ratio of inertia force to viscous force, the Weber number W_{e} denotes the ratio of inertia force to surface tension and the magnetic Reynolds number, and $R_{\mathrm{e}}^{\mathrm{mag}}$ measures the ratio of inertia force to magnetic force. The relative permeability, μ_{r}, is given by $\mu_{\mathrm{r}}=1+\chi$.

Substituting μ_{r} and the dimensionless parameters into Eq. (27), the two sides of the equation are divided by U_{c}^2, and the dimensionless dynamic equation of the MMB is obtained

$$\begin{aligned} & r_1\ddot{r}_1\left(1+\frac{n-1}{\zeta}\left(\frac{r_1}{r_2}\right)\right)+\dot{r}_1^2\left(\frac{4n-1}{2}-\frac{n-1}{2\zeta^3}\left(\frac{r_1}{r_2}\right)^3\right) \\ &= \left(1+\frac{2}{W_{\mathrm{e}}}+\frac{2\varepsilon}{\zeta W_{\mathrm{e}}}\right)\left(\frac{1}{r_1}\right)^{3\gamma}-1-A\sin\omega^* t^* \\ & -\frac{2}{r_1 W_{\mathrm{e}}}-\frac{2\varepsilon}{\zeta r_2 W_{\mathrm{e}}}-\frac{4m}{\zeta R_{\mathrm{e}}}\frac{\dot{r}_2}{r_2^2} \\ & -\frac{2l}{\zeta W_{\mathrm{e}} r_2}\left(1-\left(\frac{1}{r_2}\right)^2\right)-\frac{4}{R_{\mathrm{e}}}\left(1-\frac{1}{\zeta^3}\right)\frac{\dot{r}_1}{r_2^3 r_1} \\ & -\frac{4q}{\zeta^3}\frac{r_1^2\dot{r}_1}{r_2^3}+G_1, \end{aligned} \tag{28}$$

and

$$G_1=-\frac{9}{8R_{\mathrm{e}}^{\mathrm{mag}}}\left(\frac{k_1\left(\frac{r_1}{r_2}\right)^3+k_2\left(\frac{r_2}{r_1}\right)^3+k_3\left(\frac{r_2}{r_1}\right)^3 ln\left(\frac{r_1}{\zeta r_2}\right)+k_4}{k_5\left(\frac{r_1}{r_2}\right)^3+k_6\left(\frac{r_2}{r_1}\right)^3+k_7}\right), \tag{29}$$

where

$$\begin{aligned} k_1 &= \frac{\chi^2(3+8\chi)}{\zeta^3}, \\ k_2 &= 3\zeta^3\chi\left(12+23\chi+8\chi^2\right), \\ k_3 &= 12\zeta^3\chi(3+2\chi)^2, \\ k_4 &= -4\chi(3+4\chi)(3+2\chi), \\ k_5 &= \frac{4\chi^4}{\zeta^3}, \\ k_6 &= \zeta^3(3+\chi)^2(3+2\chi)^2, \\ k_7 &= -4\chi^2(3+\chi)(3+2\chi). \end{aligned}$$

When the oscillating magnetic field is a variable with time, its expression can be expressed as $H(t)=H_0(1+\sin(\omega_{\mathrm{m}}t))$.[18] If the changes in boundary conditions are not taken into account, the term G_1 in Eq. (28) is changed into G_2 by comparing the dynamic equation of the MMB in a steady magnetic field

$$\begin{aligned} G_2 = & -\frac{9\left(1+2\sin\left(\omega_{\mathrm{mag}}t\right)+\sin^2\left(\omega_{\mathrm{mag}}t\right)\right)}{8R_{\mathrm{e}}^{\mathrm{mag}}} \\ & \times\left(\frac{k_1\left(\frac{r_1}{r_2}\right)^3+k_2\left(\frac{r_2}{r_1}\right)^3+k_3\left(\frac{r_2}{r_1}\right)^3\ln\frac{r_1}{\zeta r_2}+k_4}{k_5\left(\frac{r_1}{r_2}\right)^3+k_6\left(\frac{r_2}{r_1}\right)^3+k_7}\right). \end{aligned} \tag{30}$$

Compared with Eq. (27), the dynamic equation of the MMB only under the acoustic field is

$$\begin{aligned} & R_1\ddot{R}_1\left[1+\left(\frac{\rho_{\mathrm{l}}-\rho_{\mathrm{s}}}{\rho_{\mathrm{s}}}\right)\frac{R_1}{R_2}\right] \\ & +\dot{R}_1^2\left[\frac{3}{2}+\left(\frac{\rho_{\mathrm{l}}-\rho_{\mathrm{s}}}{\rho_{\mathrm{s}}}\right)\left(\frac{4R_2^3-R_1^3}{2R_2^3}\right)\left(\frac{R_1}{R_2}\right)\right] \\ = & \frac{1}{\rho_{\mathrm{s}}}\left[P_{\mathrm{G0}}\left(\frac{R_{10}}{R_1}\right)^{3\gamma}-P_\infty-\frac{2\sigma_1}{R_1}-\frac{2\sigma_2}{R_2}-\frac{4\eta_{\mathrm{s0}}\dot{R}_2}{R_2^2}-\frac{2K}{R_2}\right. \\ & \left.\times\left(1-\left(\frac{R_{20}}{R_2}\right)^2\right)-4\eta_{\mathrm{S}}\frac{V_{\mathrm{S}}\dot{R}_1}{R_2^3R_1}-4\eta_{\mathrm{L}}\frac{R_1^2\dot{R}_1}{R_2^3}\right]. \end{aligned} \tag{31}$$

Substituting the dimensionless parameters into Eq. (31), the dimensionless equation is obtained only under the acoustic field

$$\begin{aligned} & r_1\ddot{r}_1\left(1+\frac{n-1}{\zeta}\left(\frac{r_1}{r_2}\right)\right)+\dot{r}_1^2\left(\frac{4n-1}{2}-\frac{n-1}{2\zeta^3}\left(\frac{r_1}{r_2}\right)^3\right) \\ = & \left(1+\frac{2}{W_{\mathrm{e}}}+\frac{2\varepsilon}{\zeta W_{\mathrm{e}}}\right)\left(\frac{1}{r_1}\right)^{3\gamma}-1-A\sin\omega^* t^* \\ & -\frac{2}{r_1 W_{\mathrm{e}}}-\frac{2\varepsilon}{\zeta r_2 W_{\mathrm{e}}}-\frac{4m}{\zeta R_{\mathrm{e}}}\frac{\dot{r}_2}{r_2^2}-\frac{2l}{\zeta W_{\mathrm{e}} r_2}\left(1-\left(\frac{1}{r_2}\right)^2\right) \\ & -\frac{4}{R_{\mathrm{e}}}\left(1-\frac{1}{\zeta^3}\right)\frac{\dot{r}_1}{r_2^3 r_1}-\frac{4q}{R_{\mathrm{e}}\zeta^3}\frac{r_1^2\dot{r}_1}{r_2^3}. \end{aligned} \tag{32}$$

3. Numerical simulations

Numerical simulations performed in this section demonstrate the dynamics characteristics of MMB's theoretical model. The simulations were carried out by using MATLAB. The parameters of R_{e} and W_{e} were presented in the reference of Malvar *et al.*[18]

3.1. Linear analysis

It was assumed that the amplitude of the MMB's radial oscillation is small, therefore the inner and outer radius can be written as

$$r_1=1+\delta(t), \quad r_2=1+\xi(t). \tag{33}$$

According to incompressible conditions, we can write

$$R_2^3-R_1^3=R_{20}^3-R_{10}^3. \tag{34}$$

Divide both sides of Eq. (34) by R_{10}^3 to obtain

$$\zeta^3(1+\xi(t))^3-(1+\delta(t))^3=\zeta^3-1. \tag{35}$$

Then we can obtain the relationship between r_2 and the small variable $\delta(t)$ as

$$r_2=1+\frac{1}{\zeta^3}\delta(t). \tag{36}$$

Substituting Eqs. (33) and (36) into Eq. (28), linearizing it and retaining the first-order term of $\delta(t)$, we can obtain the equation of the linear oscillator

$$\ddot{\delta}(t)+S\dot{\delta}(t)+\omega_0^2\delta(t) = -\frac{A\zeta\sin\omega^* t^*}{-1+n+\zeta}-\frac{9\zeta\left(k_1+k_2-k_3\ln\zeta\right)}{8R_{\mathrm{e}}^{\mathrm{mag}}\left(k_5+k_6+k_7\right)\left(-1+n+\zeta\right)}, \quad (37)$$

where the dimensionless damping constant S and the dimensionless linear resonance frequency ω_0 are given by

$$S = \frac{4\left(m+\zeta\left(\zeta^3+q-1\right)\right)}{R_{\mathrm{e}}\zeta^3\left(\zeta+n-1\right)}, \quad (38)$$

$$\omega_0 = \left(\frac{\zeta}{\zeta+n-1}\left(3\gamma\left(1+\frac{2}{W_{\mathrm{e}}}\left(1+\frac{\varepsilon}{\zeta}\right)\right)-\frac{2}{W_{\mathrm{e}}}\left(1-\frac{2l}{\zeta^4}+\frac{\varepsilon}{\zeta^4}\right)-Q\right)\right)^{1/2}, \quad (39)$$

where

$$Q=\frac{9\left(\zeta^3-1\right)\left(-k_3k_5-6k_1k_6-k_3k_6-3k_1k_7+3\left(2k_5+k_7\right)\left(k_2-k_3\ln\zeta\right)\right)}{8R_{\mathrm{e}}^{\mathrm{mag}}\zeta^3\left(k_5+k_6+k_7\right)}. \quad (40)$$

It should be noted that in Eq. (39) ω_0 is related to Q and magnetic Reynolds number $R_{\mathrm{e}}^{\mathrm{mag}}$, and it will be affected by H. To verify Eq. (39), it is substituted in $R_{\mathrm{e}}^{\mathrm{mag}}\to\infty$ and the result is

$$\omega_0 = \left(\frac{\zeta}{\zeta+n-1}\left(3\gamma\left(1+\frac{2}{W_{\mathrm{e}}}\left(1+\frac{\varepsilon}{\zeta}\right)\right)-\frac{2}{W_{\mathrm{e}}}\left(1-\frac{2l}{\zeta^4}+\frac{\varepsilon}{\zeta^4}\right)\right)\right)^{1/2}. \quad (41)$$

It is instructive to compare Eq. (41) with the dimensional resonance frequency obtained in Ref. [21]. We found that Eq. (41) can be transformed into a dimensional resonance frequency.

Figure 2 describes the resonance frequency ω_0 of MMB as the function of radius ratio ζ at four values of magnetic Reynolds numbers $R_{\mathrm{e}}^{\mathrm{mag}}$. Because of $R_{\mathrm{e}}^{\mathrm{mag}}=\frac{\rho_S U_c^2}{\mu_0 H_0^2}$, a smaller $R_{\mathrm{e}}^{\mathrm{mag}}$ corresponds to a stronger magnetic field and $H=0$ when $R_{\mathrm{e}}^{\mathrm{mag}}\to\infty$. The solid curve in Fig. 2 indicates that the resonance frequency decreases with the radius ratio ζ when the magnetic field is absent. In the meantime, $\zeta=R_{20}/R_{10}$, the larger ζ is, the thicker layer will be. It follows from above that the resonance frequency decreases with the increasing layer thickness in absent magnetic field. This is consistent with the general rule of encapsulated microbubbles. On the contrary, the resonance frequency ω_0 increases with ζ in applied magnetic field. Three dashed curves in Fig. 2 correspond to that $R_{\mathrm{e}}^{\mathrm{mag}}$ is 0.1, 1 and 10, respectively. With the increase of ζ, three dash lines have a similar increasing trend. This indicates that the magnetic field makes the resonance frequency of MMB increase and the stronger the magnetic field is, the faster the resonance frequency increases. The possible reason for these phenomenons is that the stress distribution on bubble surface was changed by magnetic field.[23] The effects of applied magnetic field is similar to an additional ambient pressure,[27] which increase the resonance frequency of MMB.

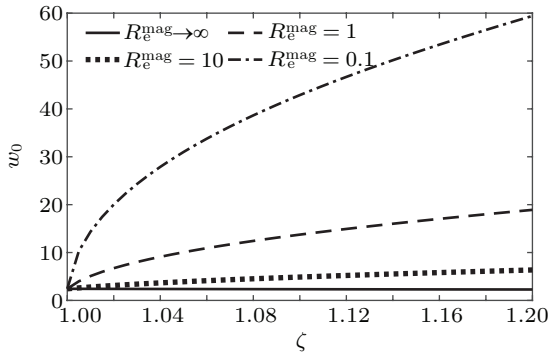


Fig. 2. Resonance frequency for an MMB as a function of radius ratio at different magnetic Reynolds number. ($W_{\mathrm{e}}=30$, $\chi=1$, $R_{\mathrm{e}}=30$, $A=0.1$, $\omega^*=1$).

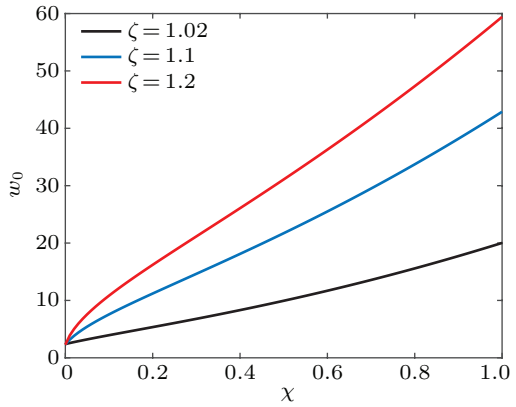


Fig. 3. Resonance frequency as a function of magnetic susceptibility. ($R_{\mathrm{e}}^{\mathrm{mag}}=0.1$, $R_{\mathrm{e}}=30$, $W_{\mathrm{e}}=30$, $\omega^*=1$, $A=0.1$).

From Eq. (39), we can also find that the resonance frequency is affected by Q and the magnetic susceptibility χ of the MF material. So the influence of susceptibility on the resonance frequency of MMB will be discussed below. Figure 3 shows that the resonance frequency ω_0 increases with χ at three larger radius ratio ζ ($\zeta=1.02$, 1.1 and 1.2) when the MMB was subjected to a steady magnetic field $R_{\mathrm{e}}^{\mathrm{mag}}=0.1$. This growth trend may be understood as that the higher magnetic susceptibility enhances the magnetic effect and produces a larger additional ambient pressure, and make the resonance frequency decrease. Significantly, for a fixed χ, ω_0 at $\zeta=1.2$

is higher than $\zeta = 1.02$ and $\zeta = 1.1$. In this case, the magnetic field and magnetization susceptibility remain constant, a possible reason for the increase of ω_0 is that the effect caused by thickening is much less than that caused by magnetic pressure.

3.2. The effect of acoustic field and static magnetic field

3.2.1. Influence of R_e^{mag}

To understand how the static magnetic field affects the oscillation of the MMB, the influence of the non-dimensional parameter R_e^{mag} was calculated at $A = 0.1$. Figure 4(a) shows the relationship of r_1–t^* under different R_e^{mag}. The radial amplitude increases with the enhancement of R_e^{mag}. Nevertheless, a strong R_e^{mag} means a weak magnetic field, so it can be said that the magnetic field retards both the expansion and contraction of the bubble. It was noted that the equilibrium radius of the oscillation also weakened as R_e^{mag} increases.

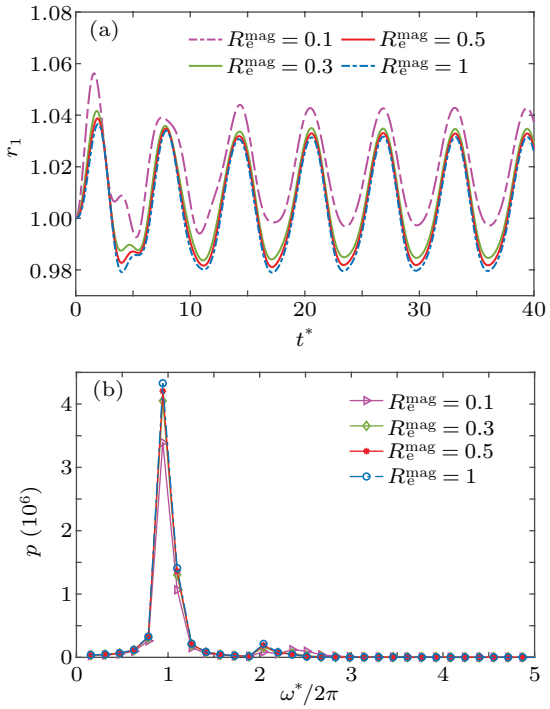


Fig. 4. Vibration graph (a) and spectrogram of the radial oscillation (b) of MMB at $R_e^{mag} = 0.1, 0.3, 0.5, 1$. ($\zeta = 1.2, A = 0.1, R_e = 30, W_e = 30, \omega^* = 1$).

To further understand how the intensity of magnetic field affects the stability and the nonlinear vibration of the MMB, it is important to analyze the frequency spectrum. Figure 4(b) shows that the resonance peak in fundamental frequency decreases as the intensity of field. There is a second harmonic and R_e^{mag} does not affect the amplitude obviously. Only in a strong magnetic field, such as $R_e^{mag} = 0.1$, the 5/2 ultraharmonic will be generated. These characteristics indicate that the existence of magnetic field suppresses the vibration of the MMB, and it is not completely stable. Malvar *et al.*[18] also observed a strong anisotropic effect on the radial oscillation of bubble in MFL and nonlinear effects caused by the unsteady expansion or contraction from transient cavitation. The amplitude is suppressed in a high-strength magnetic field, but the equilibrium radius of the microbubble would be enhanced.

The above analysis shows that the magnetic field suppresses the oscillation, so the vibration behaviors can be studied only in the presence of an external magnetic field. Figure 5 compares the vibration curves and equilibrium radius of the MMB at $\zeta = 1.02$, 1.1 and 1.2 in the same magnetic field. As a reference, the dotted line indicates the equilibrium radius in the absence of magnetic fluid. It can be seen that the magnetic field has little effect on the oscillation, and the equilibrium radius depends on ζ of the bubble. The results reveal that the bubble shows expansion and the subsequent damped oscillation when ζ is relatively large, such as $\zeta = 1.2$. On the contrary, the MMB has opposite behavior and collapses and the subsequent damped oscillation when the radius ratio is small, such as $\zeta = 1.02$ and 1.1. The subsequent damped oscillation also verifies that the magnetic field can make the oscillation more stable. Simultaneously, with increasing radius ratio, the equilibrium radius increases.

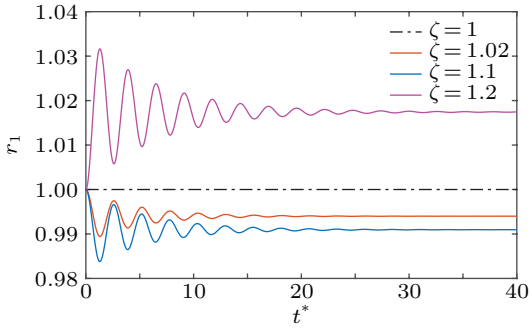


Fig. 5. Variation of radius with time in response to different ζ without the sound field ($A = 0$, $R_e^{mag} = 0.1$, $R_e = 30$, $W_e = 30$, $\omega^* = 1$).

The magnetic field deviates the equilibrium radius of the microbubble. There is no driving sound field, the magnetic field acts as damping to affect its oscillation characteristics, and the phase diagrams are shown in Fig. 6. As the energy is consumed, the amplitude of the vibrating microbubble gradually decreases. Besides, the phase trajectory is a non-closed curve and the vector diameter is a logarithmic decay. After several rotations from the starting point, the phase trajectory will tend to the center point where the equilibrium radius is located and the point is an attractor. A possible reason for the opposite direction of oscillation is that the magnetic pressure is not enough to offset the inertia pressure.[18] In fact, the MMB vibrate under the combined action of magnetic pressure and inertial pressure, and they compete with each other. If the magnetic pressure is dominant, the vibration is restrained, otherwise it is strengthened.[23]

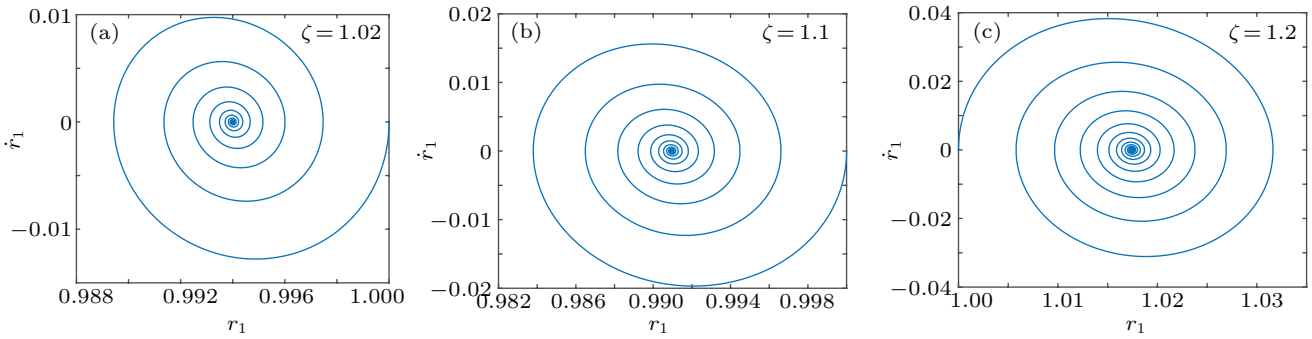


Fig. 6. MMB phase diagram in the magnetic field at $\zeta = 1.02$, 1.1, and 1.2. ($A = 0$, $R_e^{mag} = 0.1$, $R_e = 30$, $W_e = 30$, $\omega^* = 1$).

3.2.2. Influence of χ

The response of a magnetic material to an applied magnetic field is the magnetization behavior, which is generally characterized by its susceptibility. The spins of MNPs produce magnetization and change the arrangement direction, which affects their magnetic properties under the magnetic field.

Figure 7(a) demonstrates the oscillation of the MMB at three values of susceptibility. As can be seen, the maximum and minimum amplitudes are the smallest among the three sets of comparisons when $\chi = 0.1$, while they are the largest when $\chi = 0.5$. As χ increases to 1, the amplitude decreases again. At the same time, the values of χ are smaller, contributing to a decrease of equilibrium radius. The dynamic behavior may be caused by the different number of magnetic particles arranged in the direction of the magnetic field in the MFL, which leads to changes in vibration mode under the microscopic mechanism.

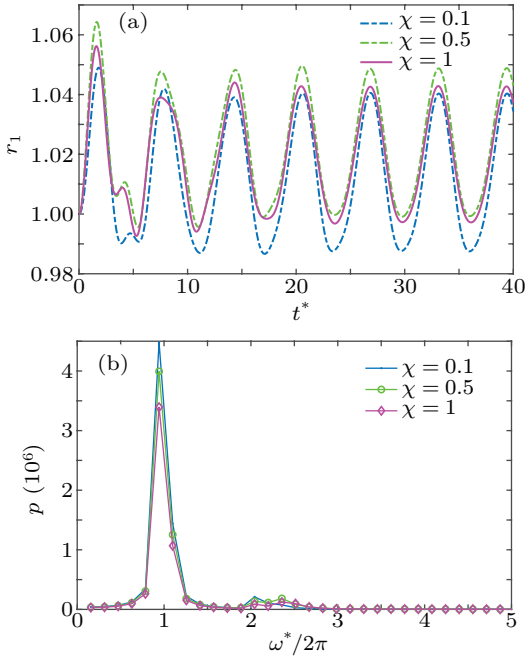


Fig. 7. Vibration graph (a) and spectrogram of the radial oscillation of MMB (b) at $\chi = 0.1$, 0.5, 1. ($\zeta = 1.2$, $A = 0.1$, $R_e = 30$, $W_e = 30$, $\omega^* = 1$, $R_e^{mag} = 0.1$).

To further discuss the influence of the magnetic susceptibility on the radial oscillation, spectrum analysis was performed in Fig. 7(b). It shows that as the magnetic susceptibility χ increases, the resonant amplitude decreases. That is to say, the increase of magnetic susceptibility inhibits the vibration. Essentially, MMB dynamics are highly dependent on the magnetic susceptibility difference between the shell material and ambient fluid. In this work, except for the material of MFL, other media are assumed to have no magnetic response and the susceptibility values were ignored. It is strictly regulated that χ used in this work is the difference of MF and surrounding medium. The result shows that the 2 and 12/5 ultra-harmonic are produced in this three cases. The second harmonic amplitude also decreases when χ increases and the largest amplitude of the 12/5 ultra-harmonic is at $\chi = 0.5$. The effect of magnetic susceptibility on nonlinear behavior is very weak.

3.3. Effect of the acoustic field

3.3.1. Influence of acoustic pressure

When the applied acoustic field parameters are unlike, the dynamic response of the MMB is also different. Figure 8 shows the behavior of the radius as a function of acoustic pressure for different values of A (0.1, 0.5, 1 and 1.5). It was noted that higher values of acoustic pressure increase the oscillation values of the radius and the unstable oscillations in the peak corresponding area becomes more obvious. In other words, greater acoustic pressure leads to the instability of the magnetic microbubble oscillation. Under acoustic waves of different intensities, although the oscillation follows the same mechanical laws, their vibration behavior is variable.

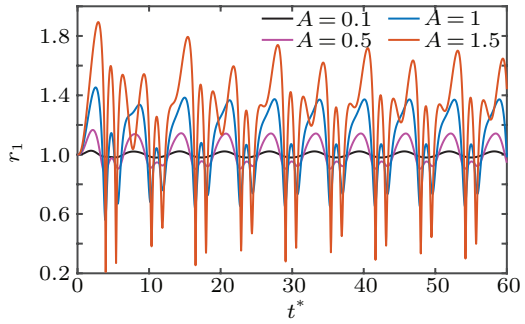


Fig. 8. The effect of acoustic pressure on MMB's vibration. ($\zeta = 1.02$, $R_e = 10$, $W_e = 20$, $\omega^* = 1$, $R_e^{mag} = 1$).

To observe the unstable response of radius oscillation under higher acoustic pressure values, the phase diagram-Poincaré cross-section diagram was taken for further analysis, as shown in Fig. 9. It shows that as the amplitude of acoustic pressure increases, the trajectory appears as numerous closed trajectories, and the shape of the trajectories is distorted from an elliptical shape. The more closed the trajectories of the microbubble, the more obvious the distortion, which indicates that the higher the energy contained and the stronger nonlinearity of the oscillation. Correspondingly, the points of the trajectory passing through the Poincaré cross-section increases from the finite point set to the infinite point set.

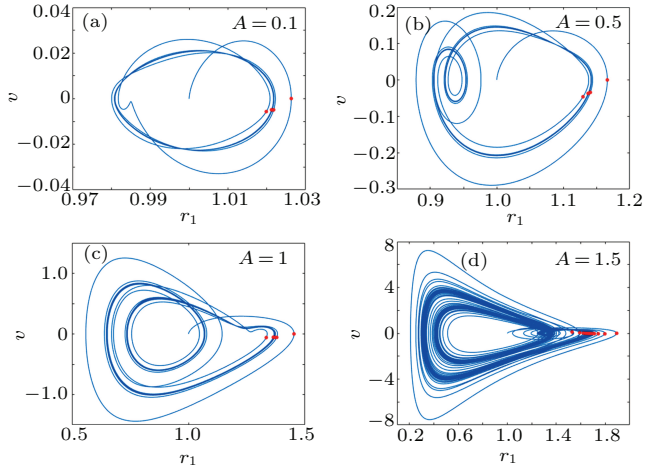


Fig. 9. The phase diagram and Poincaré cross-section (red dots) of MMB at (a) $A = 0.1$, (b) $A = 0.5$, (c) $A = 1$, (d) $A = 1.5$.

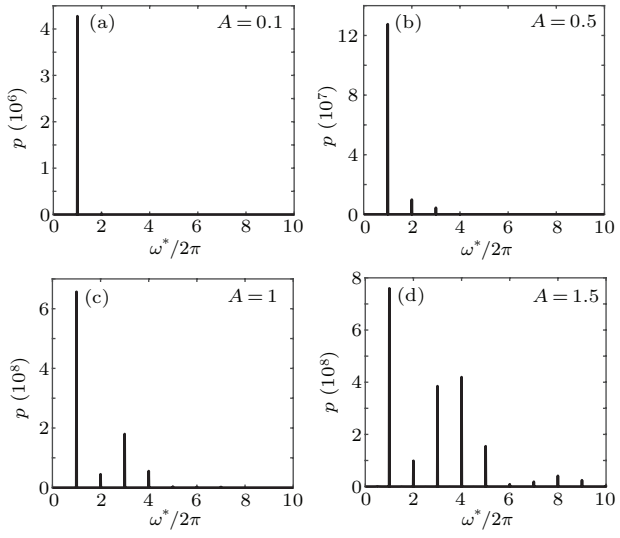


Fig. 10. The spectrum diagram of MMB at (a) $A = 0.1$, (b) $A = 0.5$, (c) $A = 1$, (d) $A = 1.5$.

Figure 10 shows the power spectrum obtained after the Fourier transform of the radius oscillation under four values of acoustic pressures. The harmonic component in the power spectrum is a sign of cavitation occurrence. As the pressure of the acoustic field increases, the resonant amplitude of fundamental frequency increases and the harmonic components increases as well. That is, when the intensity of the acoustic field is higher, the MMB absorbs more acoustic wave energy during the oscillation process, which is more conducive to cavitation. The harmonic components tend to increase with higher acoustic pressure and this means that the radius oscillation process presents stronger nonlinear vibration characteristics.

3.3.2. Influence of driving acoustic frequency

The frequency of the driving acoustic field is also an important parameter of microbubble oscillation. In Fig. 11, it is possible to show that the radius r_1 changes with normalization time t^* at four values of the acoustic frequencies tested. When other parameters remain fixed, as the acoustic frequency ω^* increases, the maximum amplitude of the transient and steady-state response radius tends to decrease. In other words, high acoustic frequency has stronger suppression on the bubble radius. To further understand how the acoustic frequency affects the radius stability, it is significant to discuss the phase space at different frequencies. As shown in Fig. 12, the most obvious phase diagram distortion occurs at the minimum acoustic frequency, and the radial amplitude and wall velocity both have the largest value. However, a higher acoustic frequency will lead a more steady oscillation state in steady-state response and nonlinear oscillation state during its transient response, respectively. Thus, the MMB has an opposite response to low-frequency and high-frequency acoustic fields such that high-frequency avoid collapse. It can be seen from Fig. 12 that the Poincaré cross-section points on the outer trajectory increase, while the points on the internal phase trajectory are concentrated, showing relative stabilization.

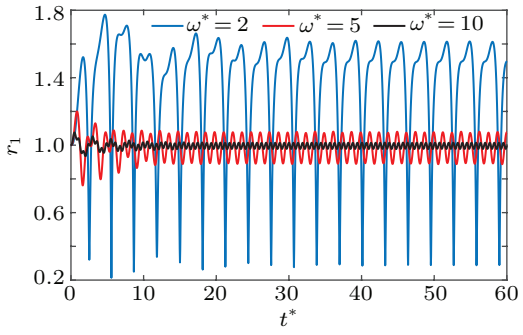


Fig. 11. The effect of acoustic frequency on radius oscillation. ($\zeta = 1.02$, $R_e = 10$, $W_e = 20$, $A = 1.5$, $R_e^{mag} = 1$).

Figure 13 shows the power spectrum of the oscillation at four frequencies of the acoustic field. It was noted that increasing the frequency of the acoustic field reduces the ultra-harmonic and increases the subharmonic components. It was observed that the radius oscillation stabilizes gradually, and the nonlinearity of the steady-state weakens.

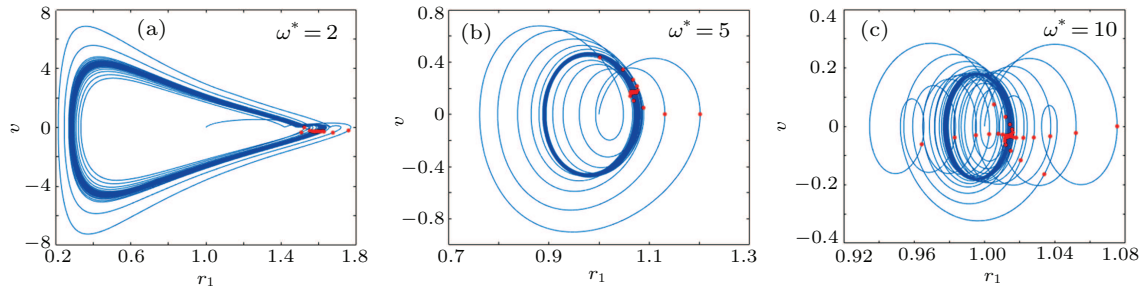


Fig. 12. The phase plot and Poincaré cross-section (red dots) of MMB at (a) $\omega^* = 2$, (b) $\omega^* = 5$, (c) $\omega^* = 10$.

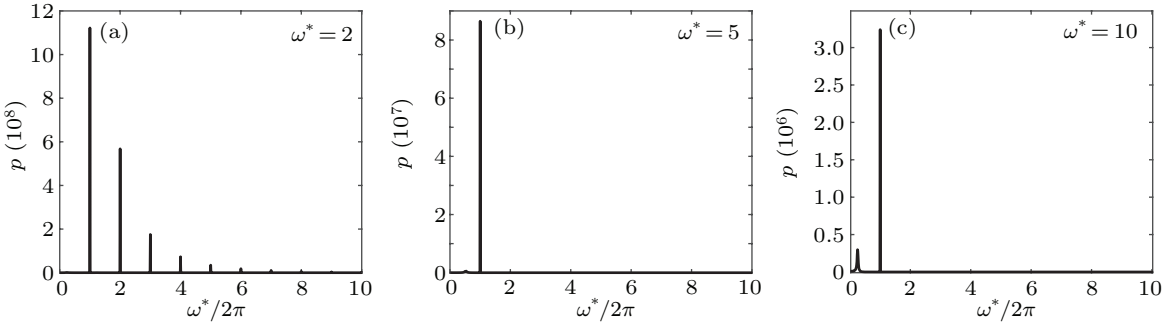


Fig. 13. The spectrum diagram of MMB at (a) $\omega^* = 2$, (b) $\omega^* = 5$, (c) $\omega^* = 10$.

3.4. The effects of the oscillatory magnetic field

Considering that the magnetic field is related to the time variable, its influence on the vibration characteristics of the microbubble is different from the steady static magnetic field. In this section, we will discuss the effects of changing magnetic field on the dynamic behavior of MMB.

3.4.1. Influence of magnetic frequency

The effects of the steady and time-varying magnetic field on the radius oscillation were studied. To explore how the combination of static and oscillating magnetic fields affects the radius oscillation, the relationship of r_1 with time t^* at three values of ω_m was studied and the results are shown in Fig. 14. When ω_m increases from 1 to 3, the amplitude has barely changed, but the vibration curves are more disorganized. The oscillation tends to be stabilized at $\omega_m = 5$ and the amplitude is minimal at this case. It is known that the higher the frequency of magnetic field is, the more stable the MMB vibration is.

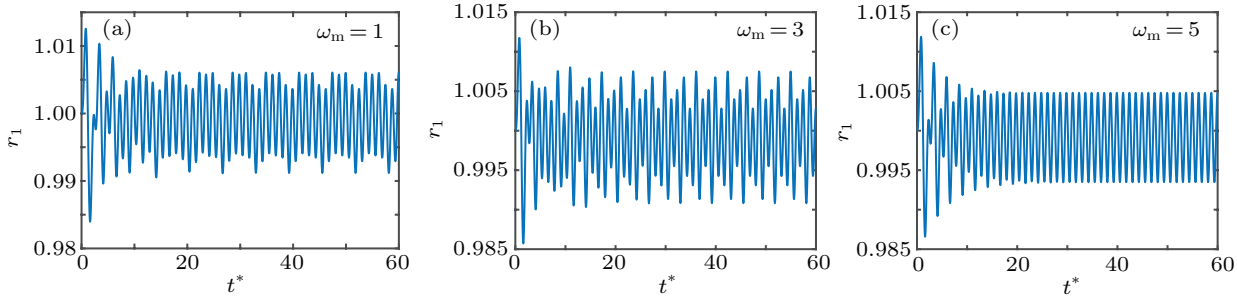


Fig. 14. The effect of ω_m on radius oscillation at $\omega_m = 1, 3, 5$. ($\omega^* = 5$, $\zeta = 1.02$, $R_e = 10$, $W_e = 20$, $A = 0.1$, $R_e^{mag} = 1$).

In this section, the nonlinear effects of MMB to a time-varying magnetic field comes into focus. In Fig. 15, the nonlinear effects of oscillating magnetic field on oscillation is more marked than a steady one. The phase trajectory is limited to a certain area, showing integral stability and local instability. The points on the Poincaré section are more scattered when $\omega_m = 3$, which is seen in Fig. 15(b). It can also be seen in Fig. 16(b) that the value corresponding to the subharmonic component becomes larger. There is also a subharmonic component when $\omega_m = 1$ (Fig. 16(a)), but its amplitude is very small. When $\omega_m = 5$ (Fig. 15(c)), the phase trajectory becomes a stable limit circle. The Poincaré cross-section points gather together, forming a line. In Fig. 16(c), there is only the fundamental frequency which implies that the magnetic microbubble does a stable periodic oscillation at this time without cavitation.

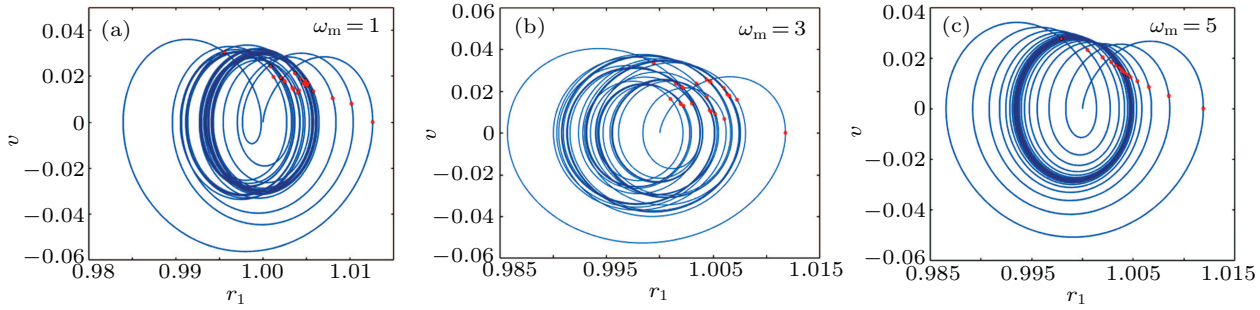


Fig. 15. The phase plot and Poincaré cross-section (red dots) of MMB at $\omega_m = 1, 3, 5$.

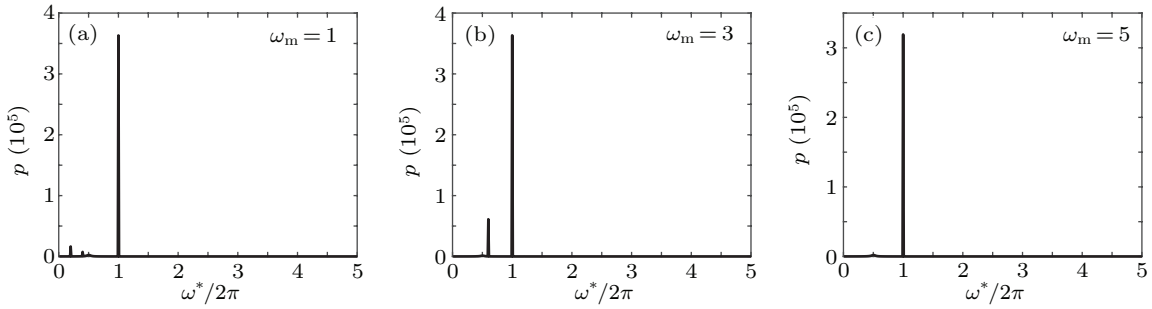


Fig. 16. The influence of different ω_m on radius oscillation at $\omega_m = 1, 3, 5$.

3.4.2. Influence of acoustic frequency

To research whether the influence of the oscillating magnetic field on radius oscillation is related to the acoustic field, the relation between r_1 and t^* is shown in Fig. 17, which is compared with the same ω_m in Fig. 14. It can be seen that the amplitude also goes up and then goes down, and reaches the maximum at $\omega_m = 3$. However, the oscillation pattern is disordered and different from that in the static magnetic field. The phase trajectory shown in Fig. 18 tends to be out of order with the increase of the acoustic frequency, and the amplitude and bubble wall velocity both decrease. The points in Poincaré section are randomly distributed, showing stronger nonlinear oscillation characteristics. Comparing the three cases of different magnetic field frequencies in Fig. 18, as ω_m increases, the phase trajectories first disperses in a certain area and then gather inward, showing a stable state. Yet, the transient response shows more nonlinearity. The points on Poincaré section change from disorder to relatively orderly arrangement. When ω_m increases to 5, the points are distributed closer to the center.

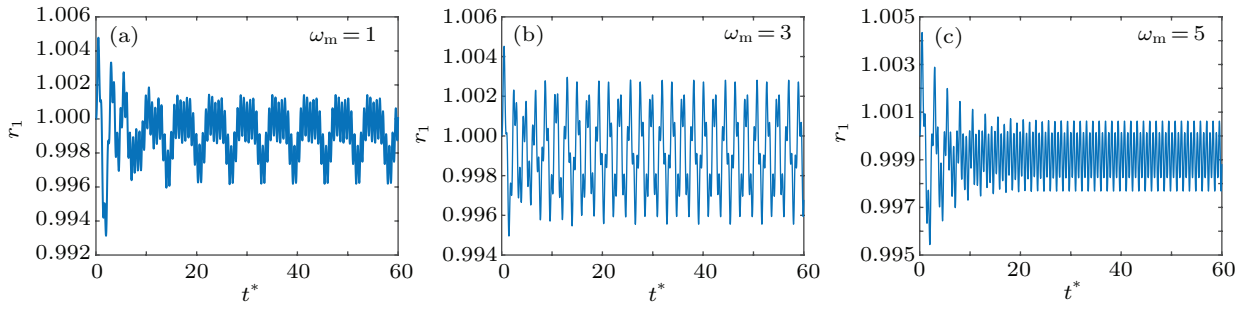


Fig. 17. The effect of ω_m on radius oscillation when $\omega^* = 10$.

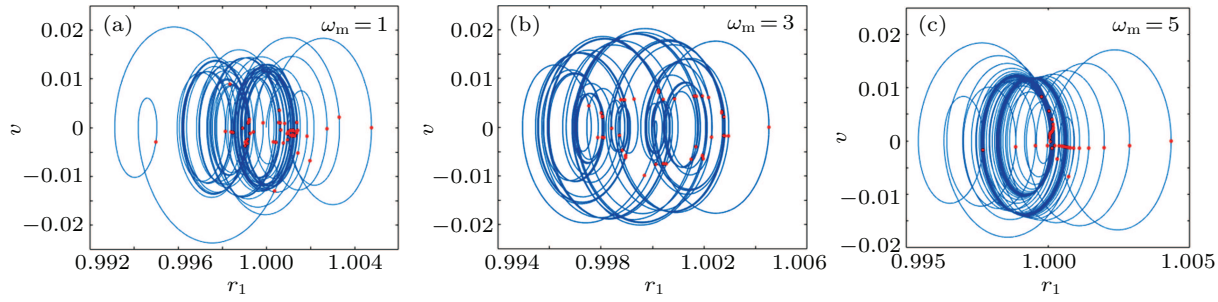


Fig. 18. The phase plot and Poincaré cross-section (red dots) of MMB at $\omega_m = 1, 3, 5$.

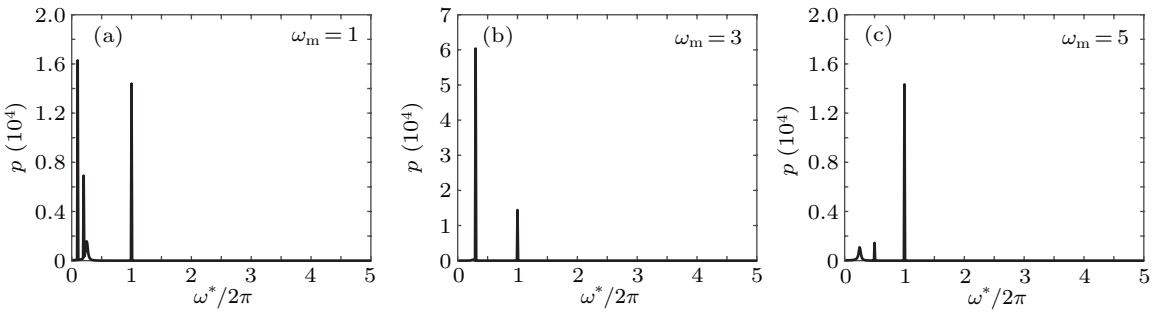


Fig. 19. The spectrum diagram of MMB at $\omega_m = 1, 3, 5$ when $\omega^* = 10$.

Compared to the power spectrums in Fig. 16, it can be seen in Fig. 19 that there are more subharmonic components when the frequency of the acoustic field ω^* is higher. Figure 19(a) shows that there are 1/10, 1/5 and 1/4 subharmonic components and the amplitude of 1/10 subharmonic is 1.13 times larger than the fundamental frequency when $\omega_m = 1$. In the case of $\omega_m = 3$ in Fig. 19(b), there is only a 3/10 subharmonic frequency, and the amplitude of subharmonic frequency is 4.19 times larger than the fundamental frequency. In Fig. 19(c), there are 1/4 and 1/2 subharmonic components, and the corresponding amplitudes of the subharmonic frequencies are 0.076 and 0.1 times of the fundamental frequency, respectively. Figure 19 illustrates the spectrum diagram of radial oscillation at three values of ω_m (1, 3 and 5). The amplitude of the fundamental frequency increases slightly when $\omega_m = 3$ and then decreases when ω_m increases to 5.

4. Conclusions

Considering the magnetic field contribution on the mechanical properties of the shell, the dynamic characteristics of MMB in a viscous fluid under acoustic and magnetic fields was investigated. An improved version of the Rayleigh–Plesset equation was formulated by considering the magnetic effects of the multi-layer microbubble dynamics. It was noted that the strength of the steady magnetic field intensity increased the resonance frequency and equilibrium radius. However, magnetic field suppressed the MMB's oscillation and generated a harmonic response. The susceptibility of the magnetic material of MFL was also high enough, the resonance frequency increased and the oscillation was suppressed. The MMB vibrated under magnetic field damping and amplitude attenuation, and the equilibrium radius was related to the radius ratio. When ζ was relatively small, the equilibrium radius was less than 1, while it was greater than 1 when ζ was large. When the acoustic pressure was higher, the oscillation was much more violent, the points passing through Poincaré cross-section and the doubled frequency components increased, and then the nonlinear characteristics were stronger.

On exploring the influence of magnetic field frequency on the vibration of the microbubble under different acoustic field, if the applied magnetic field changes with time, the influence of an time-varying magnetic field on the radius was related to the acoustic frequency. Increasing the acoustic frequency suppresses the amplitude and the velocity of the bubble wall. The transient nonlinearity response increases while that of steady-state response weakens. Furthermore, the variation of magnetic field frequency affects the vibration state and nonlinear vibration characteristics. As the frequency of the magnetic field increases, the amplitude of radius first increases and then decreases, and its subharmonic components reduce.

Acknowledgement

The authors acknowledge the support of the National Natural Science Foundation of China (Grant Nos. 12074238 and 11974232).

References

[1] Sarkar K, Shi W T, Chatterjee D and Forsberg F 2005 *J. Acoust. Soc. Am.* **118** 539
[2] Stride E, Porter C, Prieto A G and Pankhurst Q 2009 *Ultrasound Med. Bio.* **35** 861
[3] Blomley M J K, Cooke J C, Unger E C, Monaghan M J and Cosgrove D O 2001 *B. M. J* **322** 1222
[4] Vlaskou D, Mykhaylyk O and Plank C 2013 *Methods Mol. Biol.* **948** 205
[5] Zhang J, Song L M, Zhang H M, Zhou S J, Jiao Y F, Zhang X G, Zhao Y and Wang Y 2019 *Acs Omega* **4** 4691
[6] Yan L P, Miao W and Li D D 2020 *J. Nanosci. Nanotech.* **20** 6087
[7] Yang F, Li Y X, Chen Z P, Zhang Y, Wu J R and Gu N 2009 *Biomaterials* **30** 3882
[8] Zhao X, Quinto-Su P A and Ohl C D 2009 *Phys. Rev. Lett.* **102** 024501
[9] Gu Y, Chen C, Tu J, Guo X, Wu H and Zhang D 2016 *Ultrason. Sonochem.* **29** 309
[10] Young J B, Schmiedel T and Kang W 1996 *Phys. Rev. Lett.* **77** 48
[11] He W, Yang F, Wu Y H, Wen S, Chen P, Zhang Y and Gu N 2012 *Mater. Lett.* **68** 64
[12] Sciallero C, Grishenkov D, Kothapalli S V V N, Oddo L and Trucco A 2013 *J. Acoust. Soc. Am* **134** 3918
[13] Duan L, Yang F, Song L, Fang K, Tian J L, Liang Y J, Li M X, Xu N, Chen Z D, Zhang Y and Gu N 2015 *Soft Matter* **11** 5492
[14] Stride E, Owen J, Mulvana H, Pankhurst Q, Tang M and Eckersley R 2012 *J. Acoust. Soc. Am.* **131** 3245
[15] Zhang B H, Howuk K, Wu H Y, Gao Y and Jiang X N 2019 *Ultrasonics* **98** 62
[16] Owen J, Rademeyer P, Chung D, Qian C, David H, Constantin C, Peter F, Pankhurst Q A and Stride E 2015 *Interface Focus* **5** 20150001
[17] Steven J L 2014 *Phys. Fluids* **26** 061901
[18] Malvar S, Gontijo R G and Cunha F R 2018 *J. Eng. Math.* **108** 143

[19] Boev M L, Polunin V M, Ryapolov P A, Karpova G V and Prokhoro P A 2014 *Acoust. Phys.* **60** 1134
[20] Mulvana H, Eckersley R J, Tang M X, Pankhurst Q and Stride E 2012 *Ultrasound Med. Biol.* **38** 864
[21] Church C C 1995 *J. Acoust. Soc. Am.* **97** 1510
[22] Zhao L X, Mo R Y and Wang C H 2021 *Acta Phys. Sin.* **70** 014301 (in Chinese)
[23] Chen J, Zhao L X, Wang C H and Mo R Y 2021 *J. Magn. Magn. Mater* **538** 168293
[24] Hosseini S M, Ghasemi E, Fazlali A and Henneke D E 2012 *J. Nanopart. Res.* **14** 1
[25] Chen W Z 2014 *Acoustic Cavitation Physics* (Beijing: Science Press) pp. 415–417 (in Chinese)
[26] Guo S H 2008 *Electrodynamics* (3nd edn.) (Beiing: Higher Education Press) pp. 81–86 (in Chinese)
[27] Mo R Y, Wu L Y, Zhan S N and Zhang Y H 2015 *Acta Phys. Sin.* **64** 261 (in Chinese)